First examinations of ancient ferrous alloys in Renaissance armour by SR-X-Ray diffraction

Emilie Bérard, Philippe Dillmann, Solenn Réguer, Eddy Foy, Cristian Mocuta, Enrique Vega, James Braun, Caroline Toffolon-Masclet, Thomas Guilbert, Ivan Guillot

First examinations of ancient ferrous alloys in Renaissance armour by SR-X-Ray Diffraction

Bérard Emilie[1*], Dillmann Philippe[1], Réguer Solenn[2], Foy Eddy[1], Mocuta Cristian[2], Vega Enrique[1], Braun James [3], Toffolon-Masclet Caroline [4], Guilbert Thomas [4], Guillot Ivan[5]

1 Laboratoire Archéomatériaux et Prévision de l'Altération : IRAMAT UMR7065 CNRS et NIMBE UMR3685 CEA/CNRS, Université Paris-Saclay, CEA Saclay, Gif-sur-Yvette, France.
2 Synchrotron SOLEIL, Saint Aubin, France.
3 Université Paris-Saclay, CEA, DES/ISAS/DMN/SRMA/LTMEx, Gif-sur-Yvette, France.
4 Université Paris- Saclay, CEA, DES/ISAS/DMN/SRMA / LA2M, Gif-sur-Yvette, France.
5 Univ Paris Est Creteil, CNRS, ICMPE, UMR 7182, 94320 Thiais, France.

*corresponding author : eberard33@gmail.com

Abstract

The paper aims at understanding the nature of ferrous alloys used for the fabrication of Renaissance armour in a Nuremberg workshop, owned by Valentin Siebenbürger. Non-invasive techniques such as X-Ray Diffraction (XRD) using synchrotron radiation (SR) are well suited to identify the different crystalline phases, characteristic of ancient ferrous alloys, avoiding multiple sampling, rarely allowed in the case of museum pieces. However, such experiment presented analytical challenge due to the complex shape of armours. Our goal was to demonstrate the feasibility of SR-XRD measurement to identify mineral phases contained in ferrous alloys (cementite, ferrite, martensite…) on large and complete museum amour pieces and provide new insights on Renaissance armour manufacturing. The study allowed identifying phases characteristic of ancient ferrous alloys (ferrite, cementite …) but also the presence of heat treatment, on some armour plates, giving new information on manufacturing technique and workshop organization.

1. Introduction

From the late Middle Ages onwards, complete suit of armour is a complex manufactured product, composed of skilfully articulated ferrous alloys plates to fully protect its wearer. Studying the nature of metal used to make such pieces is of great interest for historical research, especially for the understanding of manufacturing techniques, including how raw materials were produced and traded [1]. To determine the structure of alloys, metallography is an efficient technique but required to collect samples on the artefacts to access localized information. Furthermore, most ancient ferrous metals being heterogeneous [2,3], it is in many cases necessary to take several samples, to be representative of the whole object [4–6]. Sampling possibilities being very limited in case of museum artefact, thus other approaches are needed.

Non-invasive methods such as diffraction techniques, using neutrons [7–11] or X-rays, are well suited to identify the different phases, characteristic of ancient ferrous alloys, such as ferrite and cementite (Fe_3C). They can also provide crucial information on the heat treatment and manufacturing techniques thanks to the study of peak shapes and broadening. With a deep penetration of neutrons into the matter (typical values around several centimetres), neutron

diffraction is a powerful tool to investigate thick samples but less suitable for examining thin sheets of metal (1 or 2 mm), such as those present in armour. In that case, X-rays diffraction (XRD), with a penetration of X-rays range up to a few hundred micrometres depending on the energy, is of great use to analyse the bulk of metal artefacts, especially using synchrotron radiation [12–15]. The specificity of synchrotron radiation (SR) presents several advantages of paramount importance. It allows a fast acquisition offering to multiply the analyses on the same artefact to assess the heterogeneity of the metal. Furthermore, the photon flux much higher than classical laboratory X-ray generator, as well as the better beam collimation and monochromaticity, improve the angular resolution and the quantification of minor phases as iron carbides (cementite) found commonly in ferrous alloys. In addition to decipher the phase composition, SR-XRD can provide information on crystallite size, residual strain and texture of the alloys, shedding light on the likely heat treatments and manufacturing techniques applied. Nevertheless, such experiment requires the possibility to move the entire object to the lab. Furthermore, it presents analytical challenge due to the complex shape of armours.
This study presents a first attempt to characterize the nature of the metal used for Renaissance armour by XRD under synchrotron radiation (later named SR-XRD) coupled with metallographic analyses on a few samples. The aim was also to provide new insights regarding ancient technical skills, identification of the metal structure and craftsmen choices, poorly documented by written sources. To shed light on these issues, five pieces of armour from the same Nuremberg workshop (Valentin Siebenbürger, Nuremberg, Germany, 16th century) have been examined for the first time.

2. Materials and methods

2.1 Samples

Five armour elements (right and left leg defence, neck defence, arm defence and gauntlet) belonging to the same complete armour (c. 1531-1535) stamped by the marks of Valentin Siebenbürger's workshop and the Nuremberg city's mark were analysed. The armour belongs to the "Musée des Beaux Arts de Rennes" (Rennes, France, Inv. n° 1096/4850 et 4851 DEP), and is currently on display at the "Musée de l'Armée" (Paris, France). SR-XRD measurements were made directly on these complete armour elements. In addition, two samples of a few millimetres have been removed from the gauntlet to be analysed by metallographic examinations to verify SR-XRD pattern interpretation made on the complete piece. Sampling was carried out using a rotary cutting tool with a diamond-coated blade.

Model alloy was also made with target carbon concentration of 0.2wt% commonly found in Renaissance armour studied, by mixing iron (high purity 99.99wt%) with a Fe-1wt%C alloy. The sample was melted 6 times to achieve good homogeneity. Carbon content was measured by combustion infrared absorption, while other minor elements using plasma emission spectrometry. Small concentrations (>0.1wt%) of Co, Mn, Ni and W were highlighted (see Table 1), attributed to minor pollutions during the melting.

Table 1 : Chemical composition of the ingot

	C	As	Cr	Co	Cu	Mn	Ni	P	Si	Ti	W	V	S
Wt%	0.19	<0.005	0.014	0.127	0.06	0.15	0.17	<0.005	0.012	<0.001	0.35	<0.005	0.0028
Uncertainy (%)	± 0,002	-	± 0,003	± 0,02	± 0,01	± 0,01	± 0,02	-	± 0,002	-	± 0,06	-	± 0,0005

Following alloys melting, samples of 8 × 8 × 2 mm3 were taken from the ingot. Then, thermal treatments were applied using a DT-1000 dilatometer. The temperature was monitored by a thermocouple constituted of 2 wires welded to the sample. The chamber was first purged three times using helium. Austenitisation was then performed in a static helium atmosphere, at 875°C during 30 min and followed by a cooling at different rates (see Table 2). The desired cooling rates were obtained by flowing helium in the chamber for rates of less than 10°C.s^{-1}. For the highest cooling rate (500°C.s^{-1}), helium previously cooled by liquid nitrogen, was injected. These thermal treatments enables to obtain various microstructures commonly found in ancient ferrous alloys, and for which SR-XRD diagrams could be compared with those acquired directly on museum pieces.

Table 2 – Cooling rates used for the fabrication of the model samples

Reference samples	Cooling rate (°C/s)
M_500	500
M_10	10
M_05	0.5

2.2 Metallographic and microhardness analyses

Samples were mounted in cross section in epoxy resin and polished using SiC abrasive papers (grade 180–4000). Final polishing was realised using Struers diamond polishing medium 3 and 1 µm, before etching with Nital 3%. Microstructures were investigated using an OLYMPUS optical microscope (model BX51). Vickers hardness of the alloys was measured using a BUEHLER VH3300 durometer with a mass of 200g held during 10 seconds. At least 10 prints were realised on each sample, followed by an average calculation.

2.3 Synchrotron X-ray diffraction

Diffractograms (intensity vs. 2θ scattering angle) were collected at the DiffAbs beamline at the Synchrotron SOLEIL using 18 keV photon energy and a hybrid pixel curved area detector (CirPAD [16], see Table 3). The X-ray spot was focused to a size of about 270 × 227 µm^2 Full Width at Half Maximum (FWHM) in respectively horizontal and vertical directions. It has to be stressed that the geometry used implies an increase of the beam footprint on the sample surface (270 × 1451 µm^2 at 9° incidence) and therefore of the area analysed (see Table 3). The total photon flux at the spot was estimated to about several 10^{11} ph.s^{-1}. CirPAD detector is composed of a batch of 20 detectors measuring simultaneously an angular range of about 135°. Calibration of the whole detector was made before the measurements to get a uniform response from all pixels and optimize the images quality. Image acquisition was fixed to 10 seconds (see Table 3). Nevertheless, a small gap is present between each detector, which prevents the acquired diffractogram from being continuous. Hence, the CirPAD was rotated

on 3 angular positions for each acquisition and the contribution of each diffractograms summed. A diffractogram without any missing data in angular range is then obtained. More data regarding calibration, data conversion and noise reduction diffractograms are available in Desjardins *et al.*[16]. To limit texture effect and increase the number of grains analysed, model alloys were spined in the beam during data acquisition.

Table 3 – SR-XRD experimental conditions

Energy (keV)	18
Wavelength (Å)	0.6888
incidence angle (°)	9
Beam size on the sample (µm)	270 × 1451
Diffraction peak angular range (°)	0-138
Acquisition time of the CirPAD (s)	10
Estimation of X-Ray attenuation length in the material (pure iron) (µm)	6

For complete piece of armour analysis, particular attention was paid to secure the analyses of the armour pieces as much as possible and to positioning and alignment of the armour pieces under the focused X-ray beam. The objects were placed in the center of DiffAbs' 6-circle diffractometer (Kappa geometry), on wide range translation stages (200mm stroke), allowing for a precise lateral positioning of the various regions of the armour pieces to be investigated (see Figure 1). This crucial step, time consuming given the complex shape of the armours, was essential to ensure the impact point on the object was placed in the centre of the diffractometer and obtain reliable data sets. Incidence angle was fixed at 9° (see Table 3). Although this angle can be verified only on plane polished samples, roughly the same beam size was expected on the armour pieces. Measurements were performed at different lateral positions on the armour. Peak identification and calculation of the FWHM were made using DIFFRAC.EVA software (BRUKER AXS) and PDF-2-2003 database (ICDD). The associated FWHM errors were estimated to be smaller than the size of the points displayed on the graphs.

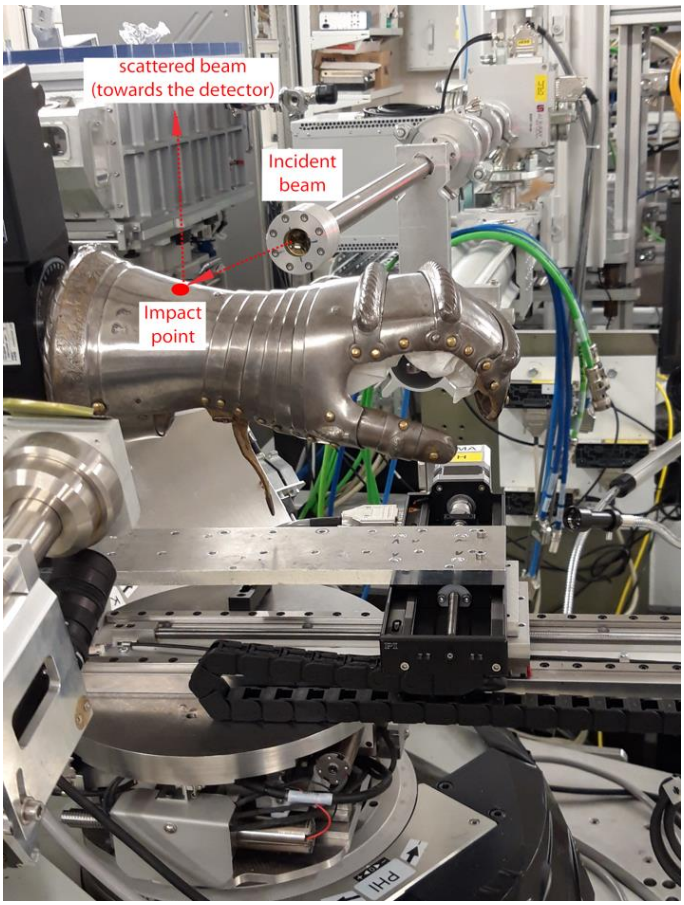

Figure 1 – Positioning of the gauntlet under the focused beam on DiffAbs beamline showing the approximate locations of impact point, incident beam and scattered beam towards the detector

3. Results

3.1 Model alloys

Microstructures of the model alloys depending on the cooling rate along with Vickers hardness average and dilatometric curves are presented in Figure 2. Quenched structures (martensite and bainite) are observed for the highest cooling rate (sample M_500, 500°C/s), while Widmanstätten ferrite microstructure is obtained for moderate cooling (sample M_10, 10°C /s), ferrite equiaxed grains and lamellar pearlite for the slowest (M_05, 0.5°C/s), close to thermodynamic equilibrium conditions. The analysis of the dilatometric curves is consistent with the observed microstructures: the samples expand during the heating phase, transform into austenite between Ac1 and Ac3, then are cooled and transform into martensite, bainite and/or ferrite and pearlite, depending of the cooling rate.

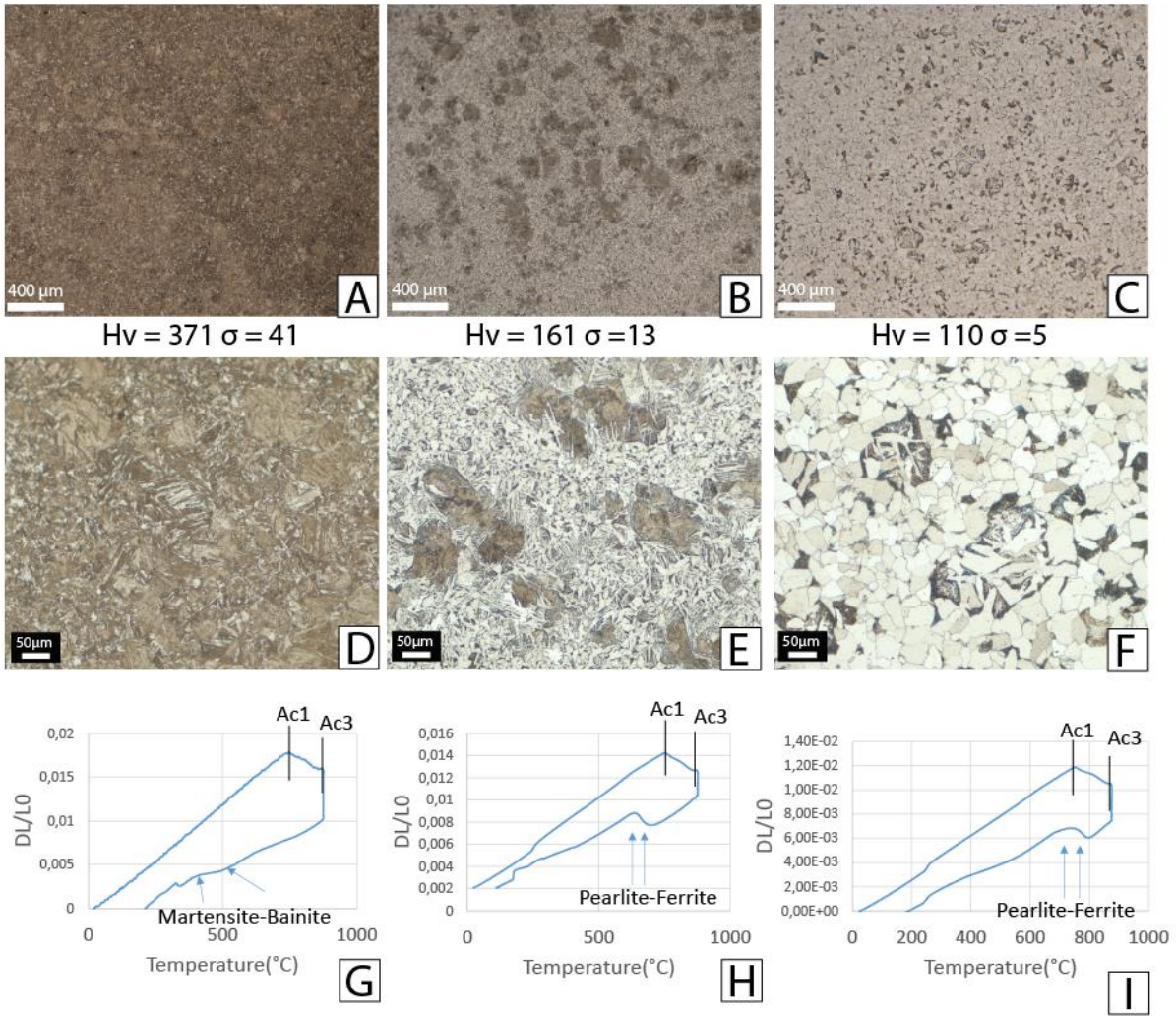

Figure 2 – « A » and « D » optical images of sample M_500 (Quenched structures martensite and bainite), « B » and « E » optical images of sample M_10 (Widmanstätten ferrite microstructure) « C » and « F » optical images of sample M_ 05 (ferrite equiaxed grains and lamellar pearlite microstructure) after Nital etching 3%. « G », « H » « I » dilatation and contraction (DL/L0) of the corresponding samples (Ac1 and Ac3: start and end transformations of α-Fe to γ-Fe).

SR-XRD diagrams are presented in Figure 3. On the zoomed view (Figure 3, B), the intensities of the 110 ferrite Bragg peak have been normalized to the same maximum height in order to facilitate comparison of peaks broadening. The difference of intensity between the cementite and ferrite peaks is high, however, cementite peak are clearly visible for samples M_10 and M_05, obtained for moderate and slow cooling rate (Figure 3, B). Furthermore, peaks of sample M_500 are broader than those derived from samples M_10 and M_05. This difference is induced by the dislocation density increase in the martensite and bainite microstructures obtained after fast cooling [17], compared to sample M_05 close to thermodynamic equilibrium. Other peaks are also present for the slowest and moderate cooling rates microstructures (M_10, M_05). We attribute it to the precipitation of manganese carbides, element whose presence is derived from the initial ingot (see Figure 3 and Table 1).

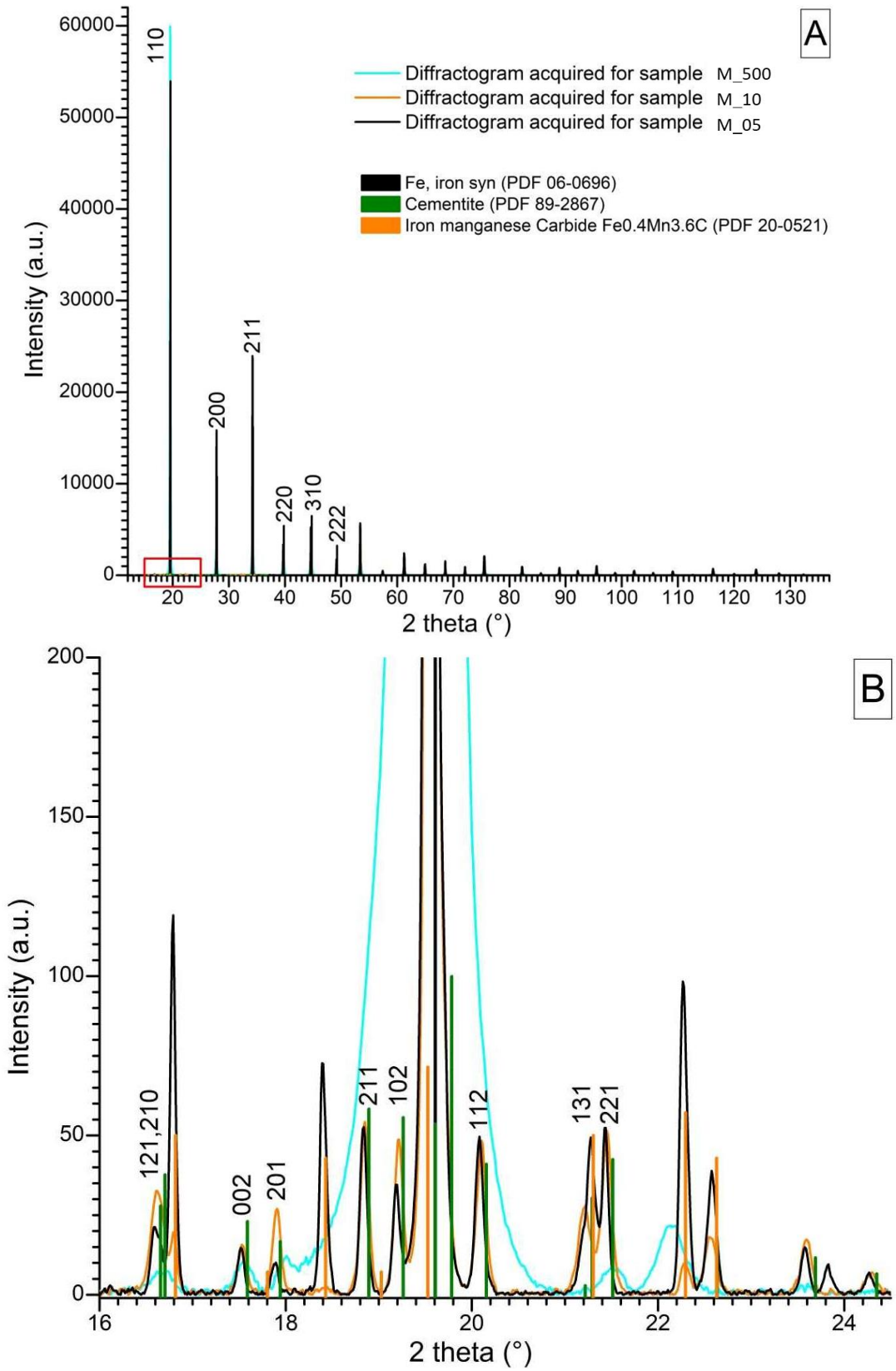

Figure 3 – « A » : Complete diffractograms of samples M_500, M_10, M_05 with identification of the main ferrite Bragg peaks « B» zoomed view with peak identification of minors phases and of the main cementite Bragg peaks; (Intensities of 110 ferrite Bragg peak normalized to the same maximum height for comparison of the apparent width factor).

Figure 4 shows a comparison between the Full Width at Half Maximum (FWHM) of the three main Bragg peaks for the three samples. The broadening effect induced by the quenching treatment is sharp

for the highest cooling rate. The difference is less pronounced between the slowest and moderate cooling rate, both samples composed of ferrite and pearlite.

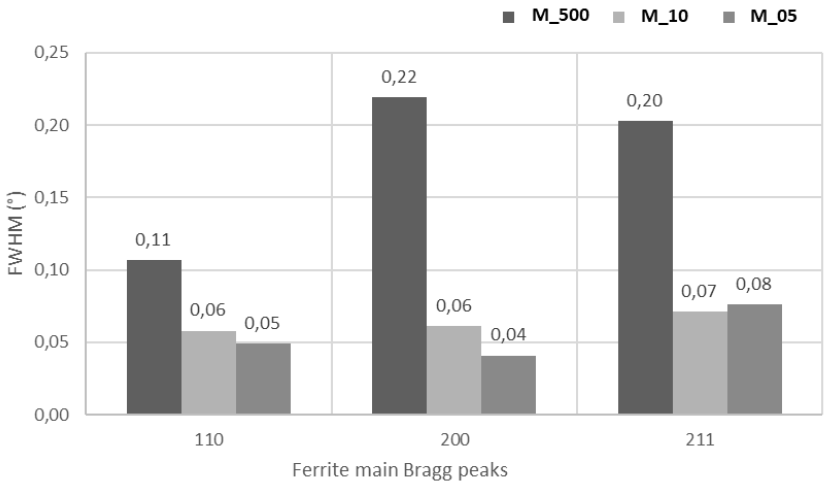

Figure 4 – Effect of peak broadening associated with the main three ferrite Bragg peaks (110, 200, 211) for samples M_500, M_10 and M_05

3.2 SR-XRD measurements on armour pieces

Two main phases were identified on armour pieces: ferrite and cementite (Fe_3C). Goethite was also encountered on a few plates (Gauntlet_pos7, Right_leg_pos1, Right_leg_pos3 and Neck_defence_pos2) due to the presence of localized corrosion products (see Figure 5). Peak shape study of the diffraction patterns provides qualitative information of the metal structure to document the artefact manufacturing techniques. Figure 5 shows the evolution of FWHM for the three main ferrite Bragg peak and diffractogram curves only for the gauntlet analysed. Results obtained on other pieces are discussed later on Figure 7 and Figure 8. As shown on Figure 5, FWHM variations illustrates a change of microstructure starting from measurement 11. Ferrite peaks are narrower for measurements 11, 12 and 13 while cementite peak intensities increase. Plates 11, 12 and 13 are most likely constituted of a ferrito-perlitic microstructure. Peak broadening on the other plates could be explained by smaller crystal size, the presence of internal stresses due to quenching treatment (as observed for reference sample M_500), or hammering of low carbon steel without subsequent annealing. Indeed, the martensitic structure obtained after quenching would not allow carbon to precipitate explaining the reduced amount of cementite. A low carbon steel hammered without final annealing would lead to similar patterns.

To confirm these assumptions, two small samples were taken at both gauntlet plates' extremities (1 and 11) and studied by metallography. Figure 6 shows the microstructure observed and allows to confirm the presence of quenched structures on plate 1. Sample Gaunt_S2, taken on plate 11 and observed perpendicularly to the surface shows a mixture of quenched structure (martensite and or bainite) displayed in two bands at the centre, and ferrite and pearlite structures at the edge. X-ray having a low penetration range (estimated around 6µm at 18keV), only the ferrite-perlitic structure located at the extremities was probed by SR-XRD, supporting the diffraction pattern interpretation.

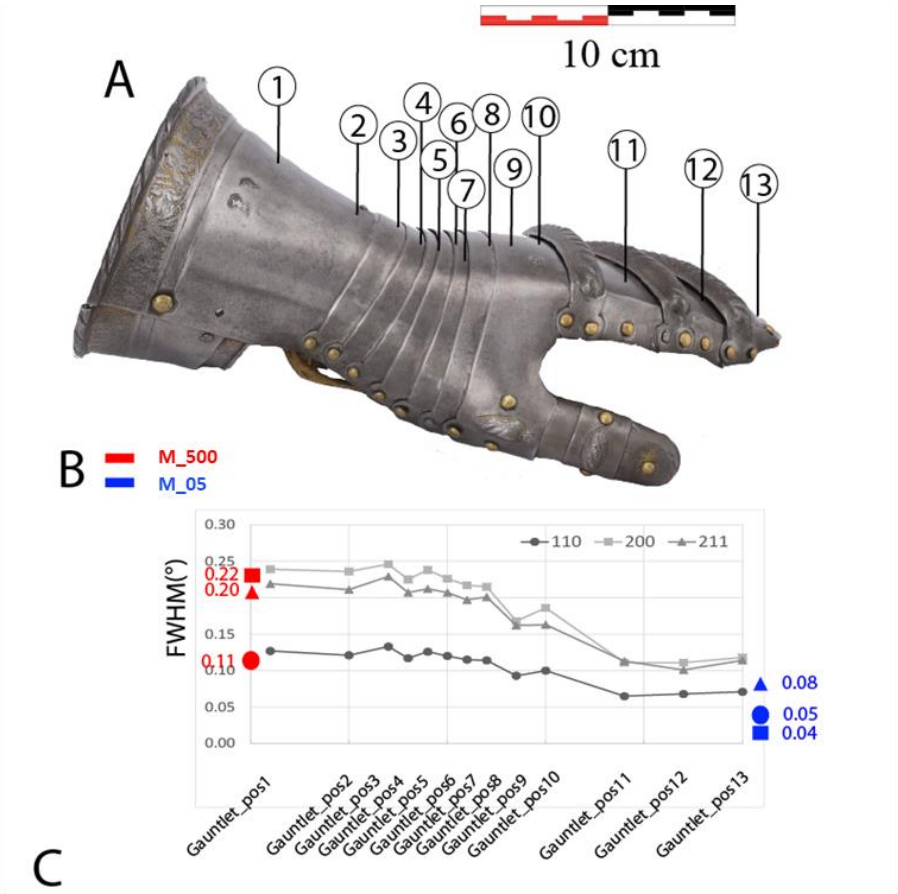

:

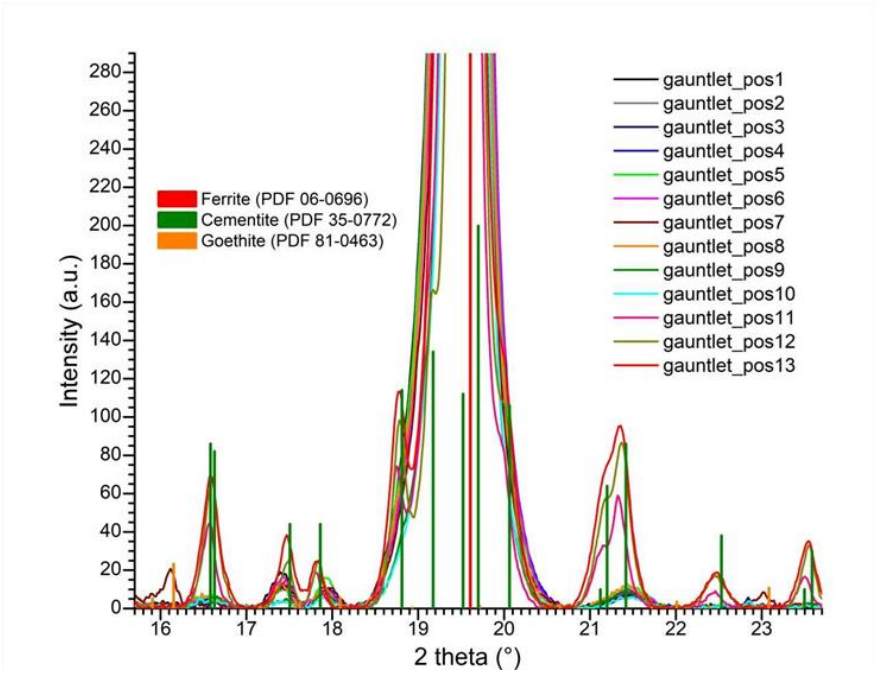

Figure 5 : « A » Localisation of the measurement on the gauntlet from the armour (Inv. n° 1096/4850 et 4851 DEP), « B » FWHM associated with the main three ferrite Bragg peaks (values obtained for samples M_1961 and M_1977 were added as reference for each ferrite Bragg peaks), « C » zoomed view of the diffractograms

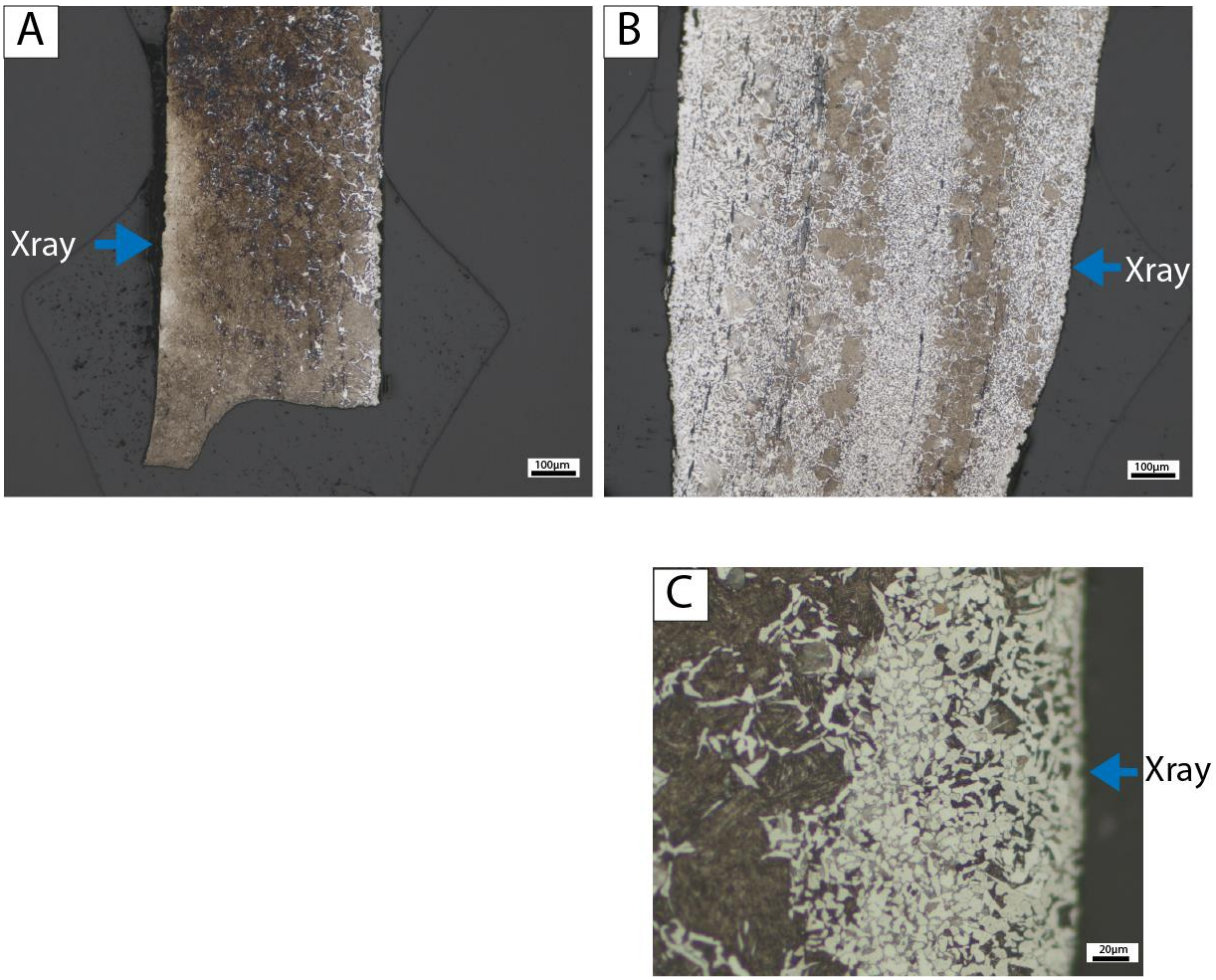

Figure 6 – Microstructures observed for samples Gaunt_S1 (A) taken on plate 1 and Gaunt_S2 (B) taken on plate 11 after Nital etching 3%, (C) zoomed view of sample Gaunt_S2

SR-XRD analyses were also made on four others armour elements. The same crystallographic phases were highlighted in all the armour pieces studied. Figure 7 shows the approximate location of the area analysed on each armour plate, while Figure 8 presents the evolution of FWHM for the three main ferrite Bragg peak for all the armour plate examined. A similar pattern interpretation to that used for the gauntlet can be applied here. Peaks broadening on Figure 8 are clearly attested for positions left leg_pos4, right leg_pos2 and the couter (arm defence_pos2). It implies that those plates were submitted to a quenching treatment or hammering of low carbon steel not followed by annealing, increasing internal stresses and therefore the hardness of the metal.

4. Discussion

On all the armour pieces studied variations intensities of ferrite peaks were frequently encountered. It could suggest a crystallographic texture of the alloys preventing a precise quantification of the different phases. Furthermore, the results raise several questions on the manufacturing techniques of the armour and the workshop organization. First, it has to be stressed that comparable FWHM evolution of some XRD peaks, suggesting similar metal structures were observed for both leg defences, and a possible choice to harden only the upper central part of the leg (see Figure 8). Furthermore, the analyses highlight variability on the metal structure (difference in cementite versus ferrite peak intensities ratios and therefore probably on carbon content and/or possibly heat treatment) at the scale of separate plates of a single armour piece and between pieces coming from the same workshop. These choices could have been made for technical reasons whereas further comparisons with armour

piece of the same type location and period would be needed to conclude. It could also suggest the implication of several craftsmen or workshops to make the complete armour, despite all the pieces being marked only by Valentin Siebenbürger's workshop. The heterogeneities observed could also indicate that the manufacturing and assemblage of all the plates, especially for the gauntlet, were not made at the same time due to a division of tasks in the workshop or possibly a later repair.

The nature of the metal and its heat treatment were essential parameters to control, ensuring the effectiveness of armour on the battlefield. According to the armourer's regulation, the city's mark applied on the pieces attested that the piece was deemed to be of sufficient quality and was stamped on piece made from a "half-steel" material [18]. Previous studies realised on small samples removed from armour bearing the marks of Nuremberg, have already suggested that various alloys, including very low carburized metal, could have been used [5,6,19,20]. The present study, which enabled to analyse most of the armour plate constituted by each armour piece, seems to confirm this trend, as it proves that different kinds of heat treatments could have been applied to the same piece or for pieces bearing the same marks. Hence, archaeometric analyses suggest a complex pattern of alloys choices, raising new issues on the understanding of written sources. Further research made on a broader number of armours may be of crucial help to shed light on these issues.

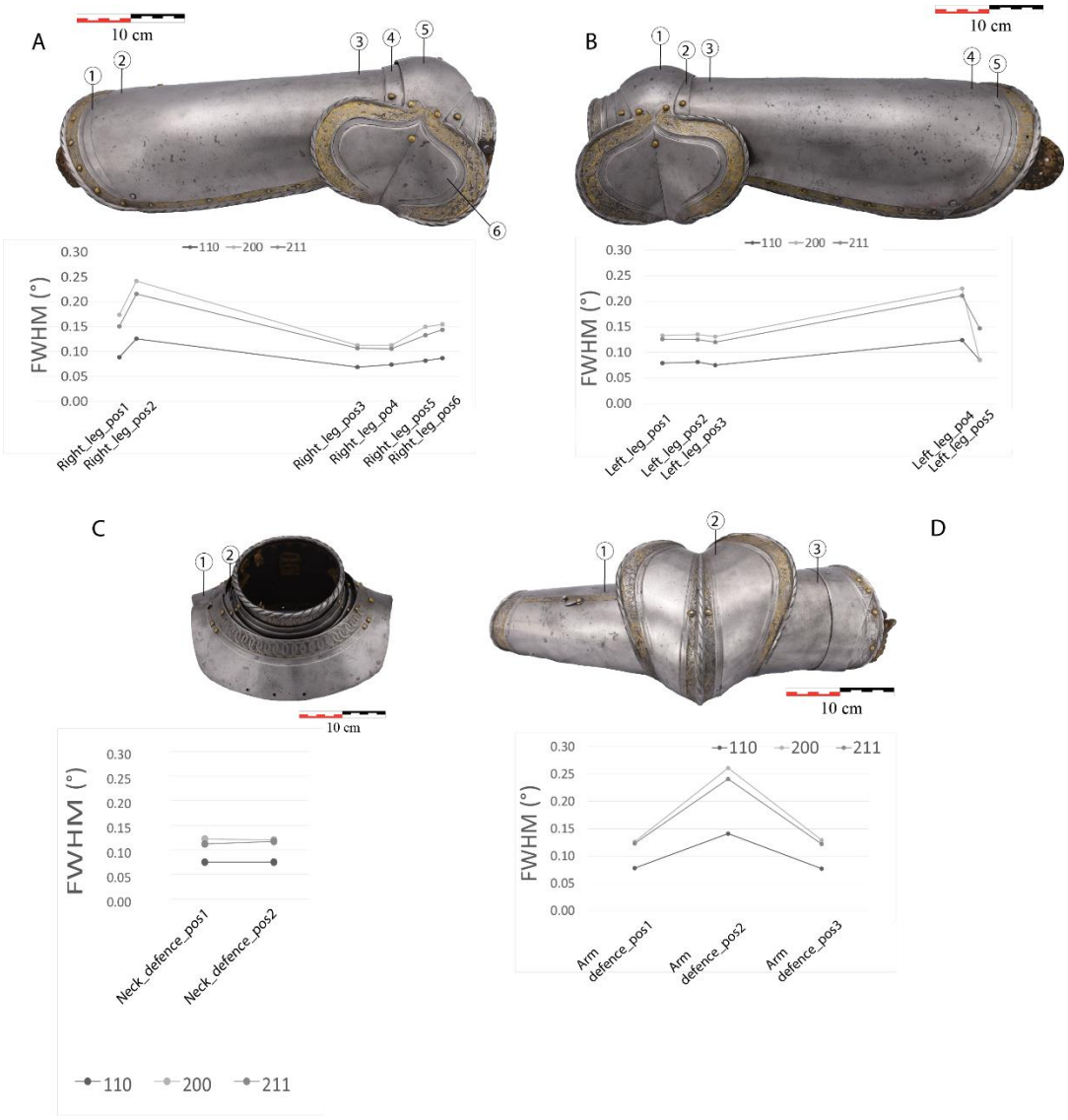

Figure 7 – Approximate location of XRD measurement made on « A » right leg, « B » left leg, « C » neck defence, « D » arm defence of the armour (Inv. n° 1096/4850 et 4851 DEP)

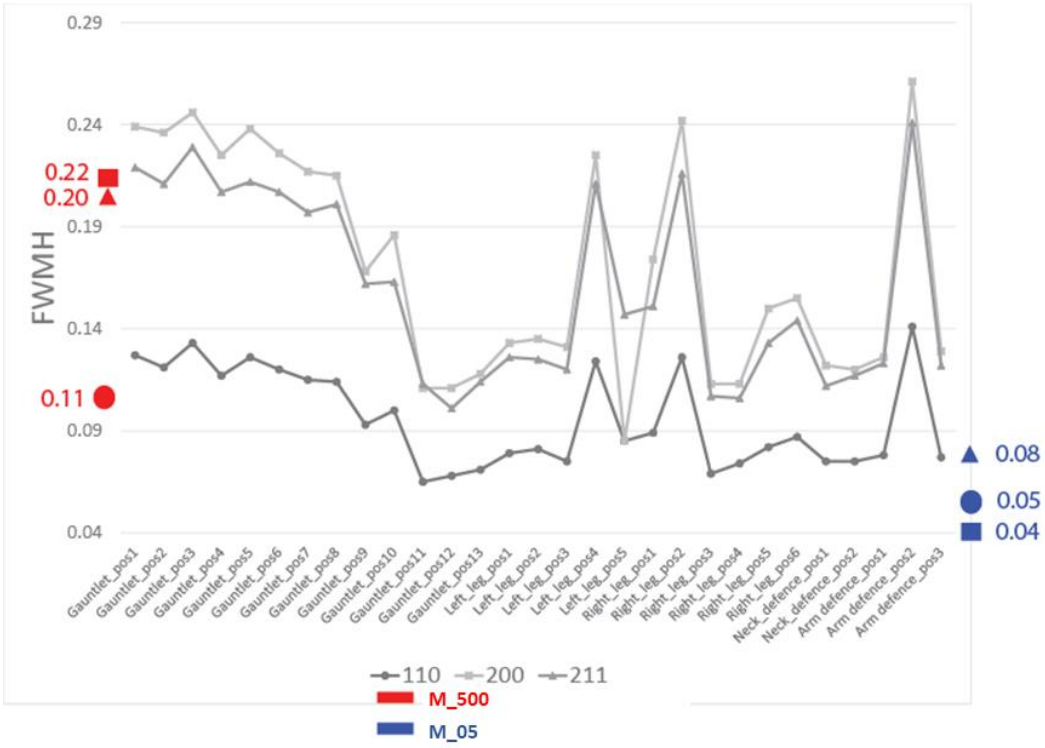

Figure 8 - FWHM associated with the main three ferrite Bragg peaks for each armour plate analysed

5. Conclusion

Sampling possibilities for Renaissance armour being very limited, the development of non-invasive and non-destructive techniques is needed. However, it presents analytical challenges due to the size and complex shape of the artefact. The present study demonstrated the feasibility and the efficiency of SR-XRD to detect the different phases of interest, including the less intense peaks of cementite phase, on five armour elements belonging to the same complete armour made in Valentin Siebenbürger's workshop. The specificity of synchrotron radiation, offering a fast acquisition, has allowed to multiply the analyses on complete museum amour piece and evidenced heterogeneities of the material used. Furthermore, the pattern interpretation highlighted the presence of quenching and/or hammering of the metal without final annealing, on some but not all the armour plates.

The developed analytical protocol is currently in progress, in particular to study the crystallographic texture of the alloys. New measurements have been made, using the available rotation carrying the CirPAD detector, to map extensive regions of the diffraction rings in angular space (up to 1/8 of sphere), in order to obtain information on sample texture, by measuring intensity variations along the diffraction rings azimuthal direction. In favourable cases, the quantitative phases analyses using the Rietveld method will allow determining the average carbon content to precise the type of alloy used.

One limitation of the present SR-XRD analyses is the low penetration of X-ray into the matter, allowing a surface analysis of only several micrometres. Ferrous alloys being often heterogeneous, a deeper penetration would improve the in depth representativeness of the results. It could be achieved, in the future, by using higher energy X-ray sources, provided that the armour elements can be moved to the

lab. Indeed, first calculations show that to reach 50 µm of X-Ray Attenuation Length a beam energy of 38 keV would be necessary.

Nevertheless, the results already obtained have permitted to highlight heterogeneities on the metal nature on separate armour plates. It raises new issues regarding the manufacturing techniques, suggesting the involvement of several craftsmen or workshops perhaps by contractual arrangement, despite the piece being stamped by one workshop. Furthermore, the developed approach opens the path to a broader non-invasive analysis of iron-based artefacts that coupled and discussed with other type of historical sources, would provide new information on ancient materials and techniques used.

References

1. M. Pfaffenbichler, *Armourers* (British Museum Press, Londres, 1992).

2. G. Pagès, P. Dillmann, P. Fluzin, and L. Long, J. Archaeol. Sci. **38**, 1234 (2011) https://doi.org/10.1016/j.jas.2010.12.017.

3. M. L'Héritier, P. Dillmann, S. Aumard, and P. Fluzin, in *World Iron*, edited by J. Humphris and T. Rehren (Archetype Publications, London, 2013), pp. 409–420.

4. E. Bérard, P. Dillmann, O. Renaudeau, C. Verna, and V. Toureille, J. Cult. Herit. **53**, 88 (2022) 10.1016/J.CULHER.2021.11.008.

5. J. Kraner, T. Lazar, B. Zorc, P. Fajfar, and M. Knap, J. Cult. Herit. **39**, 49 (2019) https://doi.org/10.1016/j.culher.2019.02.013.

6. A. Williams, *The Knight and the Blast Furnace: A History of the Metallurgy of Armour in Middle Ages and the Early Modern Period* (Brill, London, 2003).

7. F. Grazzi, L. Bartoli, F. Civita, and M. Zoppi, Anal. Bioanal. Chem. **395**, 1961 (2009) 10.1007/S00216-009-3048-6.

8. A. Fedrigo, F. Grazzi, A. Williams, A. Scherillo, F. Civita, and M. Zoppi, J. Anal. At. Spectrom. **28**, 908 (2013) 10.1039/C3JA50031D.

9. A. Fedrigo, F. Grazzi, A. R. Williams, T. Panzner, K. Lefmann, P. E. Lindelof, L. Jørgensen, P. Pentz, A. Scherillo, F. Porcher, and M. Strobl, J. Archaeol. Sci. Reports **12**, 425 (2017) https://doi.org/10.1016/j.jasrep.2017.02.014.

10. A. Fedrigo, F. Grazzi, A. Williams, S. Kabra, and M. Zoppi, J. Anal. At. Spectrom. **30**, 707 (2015) DOI https://doi.org/10.1039/C4JA00390J.

11. G. Artioli, Appl. Phys. A **89**, 899 (2007) 10.1007/s00339-007-4215-2.

12. L. Y. Marcus, Reports Prog. Phys. **75**, 36504 (2012) 10.1088/0034-4885/75/3/036504.

13. M. L. Young, F. Casadio, S. Schnepp, J. Almer, D. R. Haeffer, and D. C. Dunand, Appl. Phys. **83**, 163 (2006) https://doi.org/10.1007/s00339-006-3504-5.

14. M. L. Young, F. Casadio, J. Marvin, W. T. Chase, and D. C. Dunand, Archaeometry **52**, 1015 (2010) https://doi.org/10.1111/j.1475-4754.2009.00512.x.

15. M. G. Dowsett, P.-J. Sabbe, J. Alves Anjos, E. J. Schofield, D. Walker, P. Thomas, S. York, S. Brown, D. Wermeille, and M. Adriaens, J. Synchrotron Radiat. **27**, 653 (2020) 10.1107/S1600577520001812.

16. K. Desjardins, C. Mocuta, A. Dawiec, S. Réguer, P. Joly, J. M. Dubuisson, F. Alves, A. Noureddine, F. Bompard, and D. Thiaudière, J. Synchrotron Radiat. **29**, 180 (2022) 10.1107/S1600577521012492/GY5028SUP1.AVI.

17. P. M. Kelly, T. Maki, G. B. Olson, Z. D. Feinberg, D. Dunne, G. C. Krauss, R. Cochrane, P. J. Jacques, J. G. Speer, F. G. Caballero, C. Garcia-Mateo, B. C. De Cooman, W. Sha, M. H. F. Sluiter, M. Militzer, H. M. Urbassek, L. Sandoval, C. Capdevelia, D. Boyd, Z. Yao, M. K. Miller, S. Zaefferer, N.-N. Elhami, and S. Babu, S., *Phase Transformations in Steels* (Woodhead Publishing, Padstow, Cornwall, 2012).

18. A. F. von Reitzenstein, Waffen- Und Kostümkd. **1**, 54 (1959).

19. E. Bérard, L'armure Du XIIIe Au XVIIe Siècle En Europe : Une Approche Matérielle. Production, Nature et Circulation Du Métal, PhD thesis, Université de Cergy-Pontoise, 2019.

20. C. von Böhne, Waffen- Und Kostümkd. **1**, 47 (1961).

Funding

This work was supported by the Fondation des Sciences du Patrimoine, Paris Seine Graduate School Humanities, Creation, Heritage, Investissement d'Avenir ANR-17-EURE-0021 – Foundation for Cultural Heritage Sciences

Data availability

The datasets generated during the current study are available from the corresponding author on reasonable request

Acknowledgments

We would like to thank: François Coulon (Musée des Beaux Arts de Rennes) and Olivier Renaudeau (Musée de l'Armée) for the stimulating exchanges and allowing studying the armour, José Ferreira (Musée de l'Armée) for his help on the sampling campaigns, Dominique Thiaudière (DiffAbs beamline, Synchrotron SOLEIL) and Philippe Joly (DiffAbs beamline, Synchrotron SOLEIL), for helping to conduct the experiment and the fruitful discussions on XRD data treatment, Jean-Charles Méaudre (LAPA-IRAMAT), the staff of IPANEMA (Université Paris-Saclay, CNRS, ministère de la Culture, UVSQ, Muséum national d'histoire naturelle USR 3461), and reviewers for their useful suggestions that improved the quality of the manuscript.